SIAM J. SCI. COMPUT.
Vol. 33, No. 5, pp. 2277–2294

A HIGHER ORDER SCHEME FOR A TANGENTIALLY STABILIZED PLANE CURVE SHORTENING FLOW WITH A DRIVING FORCE*

MARTIN BALAŽOVJECH† AND KAROL MIKULA†

Abstract. We introduce a new higher order scheme for computing a tangentially stabilized curve shortening flow with a driving force represented by an intrinsic partial differential equation for an evolving curve position vector. Our new scheme is a combination of the explicit forward Euler and the fully implicit backward Euler schemes. At any discrete time step, the solution is found efficiently using a few semi-implicit iterations. Basic properties of the new scheme are proved in the paper, and its precision is tested by comparing the results with known analytical solutions. For any choice of the time step, the new higher order scheme gives exact radius of evolving uniformly discretized circles in case of flow by curvature and in case of rotation by a constant tangential velocity. Such properties do not hold for other schemes solving flow by mean curvature like the classical explicit, semi-implicit, or fully implicit schemes. In general, the scheme is second order accurate, which is shown by comparing a numerically evolving encompassed area with known analytical expression. The behavior of the scheme is discussed on representative examples, and its advantages with respect to the balance between CPU time and precision are shown.

Key words. geometric partial differential equations, evolving plane curves, curve shortening flow, tangential redistribution, driving force, higher order scheme

AMS subject classifications. 35K65, 65N40, 53C80

DOI. 10.1137/100795309

1. Introduction.

In this paper, we introduce a new higher order numerical scheme for computing the curve evolution equation

$$\partial_t \mathbf{r} = \beta \mathbf{n} + \alpha \mathbf{t}, \tag{1.1}$$

accompanied by the periodic boundary conditions. The unknown $\mathbf{r} = [x, y]$ is the position vector of an evolving curve $\Gamma = \left\{\mathbf{r}\left(u,t\right), u \in S^1, t \geq 0\right\}$, where S^1 is a circle with unit length and t is time. The arc-length parametrization along the curve Γ is given by $ds = g du$, $g = |\mathbf{r}_u|$. We shall consider velocity β in the outer normal direction in the form

$$\beta = -\varepsilon k + f, \tag{1.2}$$

where $\varepsilon > 0$ is a real parameter, k is the curvature of the curve, and $f = f(\mathbf{r})$ represents an external driving force, e.g., a velocity field projected onto the outer unit normal vector $\mathbf{n}$ of the curve or any other scalar function given in the normal direction. We use the definition of the unit tangent $\mathbf{t} = \partial_s \mathbf{r}$ and the unit normal $\mathbf{n} = \mathbf{t}^{\perp} = (\partial_s \mathbf{r})^{\perp}$, where the orthogonality relation is determined by the determinant of a matrix with columns given by $\mathbf{t}$ and $\mathbf{n}$ for which holds $\det(\mathbf{t}, \mathbf{n}) = -1$. Because of Frenet's formulas we have for the curvature vector $k\mathbf{n} = -\partial_s \mathbf{t} = -\partial_{ss} \mathbf{r}$. The velocity α in tangential direction $\mathbf{t}$ will be considered as a solution to [16, 19]

$$\partial_s \alpha = \beta k - \frac{1}{L} \int_{\Gamma} \beta k \, ds + \left(\frac{L}{g} - 1 \right) \omega, \tag{1.3}$$

*Submitted to the journal's Methods and Algorithms for Scientific Computing section May 14, 2010; accepted for publication (in revised form) May 24, 2011; published electronically September 15, 2011. This work was supported by grants APVV-0351-07, APVV-0184-10, VEGA 1/0269/09, and VEGA 1/0733/10.

http://www.siam.org/journals/sisc/33-5/79530.html

†Department of Mathematics, Slovak University of Technology, Radlinského 11, 813 68 Bratislava, Slovak Republic (balazovjech@math.sk, mikula@math.sk).

where L is the length of the curve Γ and ω is a relaxation parameter. Such tangential velocity α helps to redistribute points along the curve and stabilizes numerical computations; in the continuous formulation it has no impact on the shape of evolving closed curves. The relaxation function $\omega = \omega(t)$ controls how fast the redistribution becomes uniform. In the case $\omega = 0$, the tangential redistribution (1.3) is preserving the relative local length [10, 13, 15], while for $\omega > 0$ it gives the asymptotically uniform redistribution introduced in [16]. The reader is referred also to the papers [17, 18, 19, 23, 24], where various types of tangential velocities were considered for more general models such as nonlinear anisotropic curve shortening, motion of curves on surfaces by the geodesic curvature, fourth order curve evolutions by surface diffusion, and Willmore flow or backward mean curvature motion regularized by the Willmore flow.

Using the above-mentioned relations for the tangential, normal, and curvature vectors, we can rewrite (1.1) into the form of the following intrinsic PDE:

$$\partial_t \mathbf{r} = \varepsilon \partial_{ss} \mathbf{r} + \alpha \partial_s \mathbf{r} + f \left(\partial_s \mathbf{r}\right)^{\perp}, \tag{1.4}$$

which is, together with (1.3), discretized and solved numerically to get the unknown position vector $\mathbf{r}$. In order to solve (1.4) we introduce a new higher order Crank–Nicolson-type scheme, which is a combination of explicit forward and fully implicit backward Euler schemes. It is efficient since only a few semi-implicit iterations are necessary in the fully implicit backward Euler part. In general, the scheme is second order accurate in quantities like radius and enclosed area, which is tested by comparing with known analytical expressions. Interestingly, the new scheme gives the exact solution for the position of grid nodes in case of uniformly discretized circle shrinking by curvature (i.e., for $\varepsilon = \text{const}$, $\alpha = f = 0$), which does not hold true for any other known scheme, and it also keeps the exact radius for uniformly dicretized circle rotating by a constant tangential velocity (i.e., for $\alpha = \text{const}$, $\varepsilon = f = 0$). Such properties hold for any choice of discrete time step and are proved in the paper. For only the curve shortening flow part without tangential redistribution and without driving force, the scheme was introduced in the conference paper [2].

The curve evolution equations of the form (1.1) are used in many important applications ranging from physics to image processing [1, 22, 20, 11, 4, 12], their analysis was given, e.g., in [8, 9], and numerical schemes of different types were presented, e.g., in [6, 7, 5, 10, 13, 14, 15, 16, 19, 3]. In the next sections we present our new scheme, compare it with other known methods, and show its properties with respect to accuracy and efficiency.

2. The semidiscrete numerical scheme. If we use the space approximation of (1.4) following the ideas of the finite element or the flowing finite volume methods (cf. [6, 15, 19]), we obtain the following semidiscrete spatial discretization:

$$\frac{h_{i+1} + h_i}{2}\, \partial_t \mathbf{r}_i = \varepsilon \left(\frac{\mathbf{r}_{i+1} - \mathbf{r}_i}{h_{i+1}} - \frac{\mathbf{r}_i - \mathbf{r}_{i-1}}{h_i} \right) + \alpha_i \frac{\mathbf{r}_{i+1} - \mathbf{r}_{i-1}}{2} + f_i \mathbf{n}_i, \tag{2.1}$$

where $\mathbf{r}_i = [x_i, y_i]$, $i = 1, \ldots, n$, is a time dependent discrete solution, $h_i = |\mathbf{h}_i|$, $\mathbf{h}_i = \mathbf{r}_i - \mathbf{r}_{i-1}$ is the Euclidean distance of spatial curve representing grid points, $f_i = f(\mathbf{r}_i)$ and $\mathbf{n}_i = [n_{xi}, n_{yi}] = (\frac{\mathbf{r}_{i+1} - \mathbf{r}_{i-1}}{2})^{\perp} = [\frac{y_{i-1} - y_{i+1}}{2}, \frac{x_{i+1} - x_{i-1}}{2}]$. Because of the periodic boundary conditions we will use also the additional values defined by $\mathbf{r}_0 = \mathbf{r}_n$, $\mathbf{r}_{n+1} = \mathbf{r}_1$. Discretization of (1.3) at any time t lead to the following approximation [16, 19]:

$$\frac{\alpha_i - \alpha_{i-1}}{h_i} = \beta_{i-\frac{1}{2}} k_{i-\frac{1}{2}} - \frac{\sum_{i=1}^{n} \beta_{i-\frac{1}{2}} k_{i-\frac{1}{2}} h_i}{\sum_{i=1}^{n} h_i} + \left(\frac{\sum_{i=1}^{n} h_i}{n h_i} - 1 \right) \omega, \tag{2.2}$$

where [15]

$$k_{i-\frac{1}{2}} = \frac{\mathtt{sgn}(\det(\mathbf{h}_{i-1}, \mathbf{h}_{i+1}))}{2h_i} \arccos\left(\frac{\mathbf{h}_{i-1} \cdot \mathbf{h}_{i+1}}{h_{i-1}h_{i+1}}\right),$$

$$\beta_{i-\frac{1}{2}} = -\varepsilon k_{i-\frac{1}{2}} + f_{i-\frac{1}{2}}, \quad f_{i-\frac{1}{2}} = (f_{i-1} + f_i)/2\,. \tag{2.3}$$

One can perform time discretization of (2.1) in several different ways and obtain a first-order explicit forward Euler or first-order semi-implicit backward Euler schemes; see, e.g., [6, 15, 19]. The semi-implicit linear systems can be solved efficiently using a cyclic tridiagonal solver. Another possibility is to make a combination of fully implicit backward Euler and explicit forward Euler schemes as introduced in this paper. We show that such combination leads to higher order accuracy in all terms, i.e., in the curvature part, in the advective part related to the tangential redistribution, and in the driving force part. We will describe all above-mentioned algorithms and compare their accuracy on representative numerical examples.

3. The fully discrete numerical schemes. In all cases we approximate the time derivative $\partial_t \mathbf{r}_i$ in (2.1) by the finite difference $\frac{\mathbf{r}_i^{m+1} - \mathbf{r}_i^m}{\Delta t}$, where the index $m = 0, \ldots, M-1$ denotes discrete time stepping with a uniform time step $\Delta t = \frac{T}{M}$. The type of the scheme depends on the choice of the time approximation for all other terms in (2.1)–(2.2).

3.1. First-order explicit forward Euler scheme. It is given by

$$\frac{h_{i+1}^m + h_i^m}{2} \frac{\mathbf{r}_i^{m+1} - \mathbf{r}_i^m}{\Delta t} = \varepsilon \left(\frac{\mathbf{r}_{i+1}^m - \mathbf{r}_i^m}{h_{i+1}^m} - \frac{\mathbf{r}_i^m - \mathbf{r}_{i-1}^m}{h_i^m}\right) + \alpha_i^m \frac{\mathbf{r}_{i+1}^m - \mathbf{r}_{i-1}^m}{2} + f_i^m \mathbf{n}_i^m \tag{3.1}$$

for $i = 1, \ldots, n$ and the periodic boundary conditions $\mathbf{r}_0^m = \mathbf{r}_n^m$, $\mathbf{r}_{n+1}^m = \mathbf{r}_1^m$, with

$$\alpha_0^m = 0, \qquad \alpha_i^m = \alpha_{i-1}^m + h_i^m \beta_{i-\frac{1}{2}}^m k_{i-\frac{1}{2}}^m - h_i^m \frac{\sum_{i=1}^n \beta_{i-\frac{1}{2}}^m k_{i-\frac{1}{2}}^m h_i^m}{\sum_{i=1}^n h_i^m} + \left(\frac{\sum_{i=1}^n h_i^m}{n} - h_i^m\right) \omega^m. \tag{3.2}$$

Here $\mathbf{r}_i^m = [x_i^m, y_i^m]$ represents the coordinates of the position vector of all nodes at the discrete time $t^m = m\Delta t$ and

$$h_i^m = \sqrt{(x_i^m - x_{i-1}^m)^2 + (y_i^m - y_{i-1}^m)^2}, \qquad f_i^m = f(\mathbf{r}_i^m)\,,$$
$$\mathbf{n}_i^m = [n_{xi}^m, n_{yi}^m] = \left[\frac{y_{i-1}^m - y_{i+1}^m}{2}, \frac{x_{i+1}^m - x_{i-1}^m}{2}\right].$$

From (3.1) we can see that the new position vector $\mathbf{r}_i^{m+1} = [x_i^{m+1}, y_i^{m+1}]$ in the next time step $t^{m+1} = (m+1)\Delta t$ is given by

$$\mathbf{r}_i^{m+1} = \mathbf{r}_i^m + \frac{2\Delta t}{h_{i+1}^m + h_i^m} \left(\varepsilon \left(\frac{\mathbf{r}_{i+1}^m - \mathbf{r}_i^m}{h_{i+1}^m} - \frac{\mathbf{r}_i^m - \mathbf{r}_{i-1}^m}{h_i^m}\right) + \alpha_i^m \frac{\mathbf{r}_{i+1}^m - \mathbf{r}_{i-1}^m}{2} + f_i^m \mathbf{n}_i^m\right). \tag{3.3}$$

3.2. First-order semi-implicit backward Euler scheme. In this case we consider the system

$$\frac{h_{i+1}^m + h_i^m}{2}\frac{\mathbf{r}_i^{m+1} - \mathbf{r}_i^m}{\Delta t} = \varepsilon\left(\frac{\mathbf{r}_{i+1}^{m+1} - \mathbf{r}_i^{m+1}}{h_{i+1}^m} - \frac{\mathbf{r}_i^{m+1} - \mathbf{r}_{i-1}^{m+1}}{h_i^m}\right) + \alpha_i^m \frac{\mathbf{r}_{i+1}^{m+1} - \mathbf{r}_{i-1}^{m+1}}{2} + f_i^m \mathbf{n}_i^m, \tag{3.4}$$

for $i = 1, \ldots, n$ and periodic boundary conditions $\mathbf{r}_0^{m+1} = \mathbf{r}_n^{m+1}$, $\mathbf{r}_{n+1}^{m+1} = \mathbf{r}_1^{m+1}$, with α_i^m, f_i^m, and $\mathbf{n}_i^m$ given as in the explicit scheme. The new coordinates of the position vector $\mathbf{r}_i^{m+1}$ are thus determined by solving the cyclic tridiagonal system

$$\left(\frac{\alpha_i^m}{2} - \frac{\varepsilon}{h_i^m}\right)\mathbf{r}_{i-1}^{m+1} + \left(\frac{h_{i+1}^m + h_i^m}{2\Delta t} + \frac{\varepsilon}{h_{i+1}^m} + \frac{\varepsilon}{h_i^m}\right)\mathbf{r}_i^{m+1} + \left(-\frac{\alpha_i^m}{2} - \frac{\varepsilon}{h_{i+1}^m}\right)\mathbf{r}_{i+1}^{m+1} = \frac{h_{i+1}^m + h_i^m}{2\Delta t}\mathbf{r}_i^m + f_i^m \mathbf{n}_i^m, \quad i = 1, \ldots, n. \tag{3.5}$$

Remark 1. The solution of the linear system (3.5), and all linear systems arising in the numerical schemes presented later in this paper, is obtained by the so-called cyclic tridiagonal solver (see, e.g., [21]), which is a generalization of the standard Thomas algorithm to a tridiagonal matrices with additional nonzero entries at corners. Such method has $O(n)$ complexity so it is fast, and a sufficient (not necessary) condition for its numerical stability and unique solvability of the system (3.5) is a strict diagonal dominance of the system matrix. It is easy to see that such property is achieved by a choice of time step fulfilling the condition

$$\Delta t < \frac{1}{2}\frac{h_{i+1}^m + h_i^m}{|\frac{\varepsilon}{h_i^m} - \frac{\alpha_i^m}{2}| + |\frac{\varepsilon}{h_{i+1}^m} + \frac{\alpha_i^m}{2}| - (\frac{\varepsilon}{h_i^m} + \frac{\varepsilon}{h_{i+1}^m})}, \qquad i = 1, \ldots, n, \tag{3.6}$$

so it is worthwhile to check such a condition before solving the system and to adjust the time step accordingly. On the other hand, it is known that the tridiagonal solver is more robust than assumed in theory [21], so one can also use larger time steps, if no numerical instability arises in computational experiment.

3.3. First-order fully implicit backward Euler scheme. It is given by the (nonlinear) system of equations

$$\frac{h_{i+1}^{m+1} + h_i^{m+1}}{2}\frac{\mathbf{r}_i^{m+1} - \mathbf{r}_i^m}{\Delta t} = \varepsilon\left(\frac{\mathbf{r}_{i+1}^{m+1} - \mathbf{r}_i^{m+1}}{h_{i+1}^{m+1}} - \frac{\mathbf{r}_i^{m+1} - \mathbf{r}_{i-1}^{m+1}}{h_i^{m+1}}\right) + \alpha_i^{m+1} \frac{\mathbf{r}_{i+1}^{m+1} - \mathbf{r}_{i-1}^{m+1}}{2} + f_i^{m+1} \mathbf{n}_i^{m+1}, \tag{3.7}$$

$i = 1, \ldots, n$, and periodic boundary conditions, where

$$\alpha_0^{m+1} = 0, \qquad \alpha_i^{m+1} = \alpha_{i-1}^{m+1} + h_i^{m+1}\beta_{i-\frac{1}{2}}^{m+1}k_{i-\frac{1}{2}}^{m+1} - h_i^{m+1}\frac{\sum_{i=1}^n \beta_{i-\frac{1}{2}}^{m+1}k_{i-\frac{1}{2}}^{m+1}h_i^{m+1}}{\sum_{i=1}^n h_i^{m+1}} + \left(\frac{\sum_{i=1}^n h_i^{m+1}}{n} - h_i^{m+1}\right)\omega^{m+1}. \tag{3.8}$$

In this scheme we use distances of nodes h_i^{m+1}, tangential velocity α_i^{m+1}, normal velocity $\beta_{i-\frac{1}{2}}^{m+1}$, curvature $k_{i-\frac{1}{2}}^{m+1}$, and normals $\mathbf{n}_i^{m+1}$ at the time level $t^{m+1} = (m+1)\,\Delta t$. To obtain h_i^{m+1}, α_i^{m+1}, $\beta_{i-\frac{1}{2}}^{m+1}$, $k_{i-\frac{1}{2}}^{m+1}$, and $\mathbf{n}_i^{m+1}$ we solve iteratively the following semi-implicit cyclic tridiagonal system:

$$\begin{aligned}(3.9)\quad &\left(\frac{\alpha_i^{m(l)}}{2} - \frac{\varepsilon}{h_i^{m(l)}}\right)\mathbf{r}_{i-1}^{m(l+1)} - \left(\frac{\alpha_i^{m(l)}}{2} + \frac{\varepsilon}{h_{i+1}^{m(l)}}\right)\mathbf{r}_{i+1}^{m(l+1)} \\ &\qquad + \left(\frac{h_{i+1}^{m(l)} + h_i^{m(l)}}{2\Delta t} + \frac{\varepsilon}{h_{i+1}^{m(l)}} + \frac{\varepsilon}{h_i^{m(l)}}\right)\mathbf{r}_i^{m(l+1)} \\ &\qquad\qquad = \frac{h_{i+1}^{m(l)} + h_i^{m(l)}}{2\Delta t}\mathbf{r}_i^m + f_i^{m(l)}\mathbf{n}_i^{m(l)}\end{aligned}$$

with iteratively updated coefficients

$$(3.10)\quad h_i^{m(l)} = \sqrt{(x_i^{m(l)} - x_{i-1}^{m(l)})^2 + (y_i^{m(l)} - y_{i-1}^{m(l)})^2}, \qquad f_i^{m(l)} = f(\mathbf{r}_i^{m(l)})$$

$$\begin{aligned}(3.11)\quad &\alpha_0^{m(l)} = 0\,, \qquad \alpha_i^{m(l)} = \alpha_{i-1}^{m(l)} + h_i^{m(l)}\beta_{i-\frac{1}{2}}^{m(l)}k_{i-\frac{1}{2}}^{m(l)} - h_i^{m(l)}\frac{\sum_{i=1}^n \beta_{i-\frac{1}{2}}^{m(l)}k_{i-\frac{1}{2}}^{m(l)}h_i^{m(l)}}{\sum_{i=1}^n h_i^{m(l)}} \\ &\qquad\qquad + \left(\frac{\sum_{i=1}^n h_i^{m(l)}}{n} - h_i^{m(l)}\right)\omega^{(m+1)}\,,\end{aligned}$$

$$(3.12)\quad \mathbf{n}_i^{m(l)} = \left[\frac{y_{i-1}^{m(l)} - y_{i+1}^{m(l)}}{2}, \frac{x_{i+1}^{m(l)} - x_{i-1}^{m(l)}}{2}\right]$$

for $l = 0, 1, 2, \ldots$. The system is solved by a cyclic tridiagonal solver as discussed in Remark 1 (the condition (3.6) should be checked in every lth iteration), and the iterative process is stopped if the difference in length of two consecutive curves is less than a prescribed tolerance, i.e., $|L^{m(l)} - L^{m(l+1)}| \le TOL$. Since the length of the curve is computed inside the algorithm, the evaluation of the stopping criterion is straightforward and does not increase the CPU time. For sufficiently small TOL we use the last solution $\mathbf{r}_i^{m(l+1)}$, $i = 1, \ldots, n$, as the approximation of $\mathbf{r}_i^{m+1}$, the solution of the scheme at time level $(m+1)\Delta t$.

3.4. The higher order scheme. It is a combination of (3.1) and (3.7); namely, we solve the system of equations

$$\begin{aligned}(3.13)\quad &\frac{h_{i+1}^m + h_i^m + h_{i+1}^{m+1} + h_i^{m+1}}{2}\frac{\mathbf{r}_i^{m+1} - \mathbf{r}_i^m}{\Delta t} \\ &\qquad = \varepsilon\left(\frac{\mathbf{r}_{i+1}^m - \mathbf{r}_i^m}{h_{i+1}^m} - \frac{\mathbf{r}_i^m - \mathbf{r}_{i-1}^m}{h_i^m}\right) + \alpha_i^m\frac{\mathbf{r}_{i+1}^m - \mathbf{r}_{i-1}^m}{2} + f_i^m\mathbf{n}_i^m \\ &\quad + \varepsilon\left(\frac{\mathbf{r}_{i+1}^{m+1} - \mathbf{r}_i^{m+1}}{h_{i+1}^{m+1}} - \frac{\mathbf{r}_i^{m+1} - \mathbf{r}_{i-1}^{m+1}}{h_i^{m+1}}\right) + \alpha_i^{m+1}\frac{\mathbf{r}_{i+1}^{m+1} - \mathbf{r}_{i-1}^{m+1}}{2} + f_i^{m+1}\mathbf{n}_i^{m+1},\end{aligned}$$

$i = 1, \ldots, n$ and periodic boundary conditions. In order to determine the solution $\mathbf{r}_i^{m+1}, i = 1, \ldots, n$, we iteratively solve the following semi-implicit cyclic tridiagonal

linear system:

$$
\begin{aligned}
(3.14)\quad &\left(\frac{h_{i+1}^{m(l)}+h_i^{m(l)}+h_{i+1}^m+h_i^m}{2\Delta t}+\frac{\varepsilon}{h_{i+1}^{m(l)}}+\frac{\varepsilon}{h_i^{m(l)}}\right)\mathbf{r}_i^{m(l+1)}\\
&\quad+\left(\frac{\alpha_i^{m(l)}}{2}-\frac{\varepsilon}{h_i^{m(l)}}\right)\mathbf{r}_{i-1}^{m(l+1)}-\left(\frac{\alpha_i^{m(l)}}{2}+\frac{\varepsilon}{h_{i+1}^{m(l)}}\right)\mathbf{r}_{i+1}^{m(l+1)}\\
&\quad=\left(\frac{h_{i+1}^{m(l)}+h_i^{m(l)}+h_{i+1}^m+h_i^m}{2\Delta t}-\frac{\varepsilon}{h_{i+1}^m}-\frac{\varepsilon}{h_i^m}\right)\mathbf{r}_i^m\\
&\quad-\left(\frac{\alpha_i^m}{2}-\frac{\varepsilon}{h_i^m}\right)\mathbf{r}_{i-1}^m+\left(\frac{\alpha_i^m}{2}+\frac{\varepsilon}{h_{i+1}^m}\right)\mathbf{r}_{i+1}^m+f_i^m\mathbf{n}_i^m+f_i^{m(l)}\mathbf{n}_i^{m(l)}
\end{aligned}
$$

with coefficients update given by (3.10)–(3.12). The system is solved by the cyclic tridiagonal solver using an analogy of the condition (3.6) given by

$$
(3.15)\qquad \Delta t<\frac{1}{2}\frac{h_{i+1}^m+h_i^m+h_{i+1}^{m(l)}+h_i^{m(l)}}{|\frac{\varepsilon}{h_i^{m(l)}}-\frac{\alpha_i^{m(l)}}{2}|+|\frac{\varepsilon}{h_{i+1}^{m(l)}}+\frac{\alpha_i^{m(l)}}{2}|-(\frac{\varepsilon}{h_i^{m(l)}}+\frac{\varepsilon}{h_{i+1}^{m(l)}})},\qquad i=1,\dots,n\,,
$$

which is worth checking in every iteration. The iterative process is stopped by the same criterion as in the case of the fully implicit scheme.

THEOREM 3.1. *Let us consider the curve shortening flow problem, i.e., the equation* (1.4) *with* $f=0$, $\alpha=0$, *and* $\varepsilon>0$, *for the initial uniformly discretized circle. Then the higher order scheme* (3.13) *gives the exact solution (i.e., exact position of grid nodes) in every discrete time step with arbitrary choice of time step length* Δt.

Proof. Let the initial uniformly discretized circle be given by the complex numbers $\mathbf{r}_i^0=x_i^0+\mathbb{i}y_i^0=r^0(\cos\varphi_i+\mathbb{i}\sin\varphi_i)=r^0e^{\mathbb{i}\varphi_i}$, $\varphi_i=i\varphi$, $\varphi=2\pi/n$, $i=1,\dots,n$, $\mathbb{i}=\sqrt{-1}$, and without losing generality let $\varepsilon=1$.

Let us have any regular cyclic tridiagonal matrix with diagonal coefficient equal to a and upper and lower diagonal coefficients equal to b, where a and b are given constants. By simple calculations

$$
be^{\mathbb{i}\varphi_{i-1}}+ae^{\mathbb{i}\varphi_i}+be^{\mathbb{i}\varphi_{i+1}}=\left(a+be^{-\mathbb{i}\varphi}+be^{\mathbb{i}\varphi}\right)e^{\mathbb{i}\varphi_i}=(a+2b\cos\varphi)e^{\mathbb{i}\varphi_i},
$$

we get that x and y coordinates of a uniformly discretized circle form the eigenspace of such matrices with the common eigenvalue $(a+2b\cos\varphi)$.

Let us take any time step m and assume uniform distribution of grid points, i.e., $h_i^m=h^m$. Then let us also assume that $h_i^{m(l)}=h^{m(l)}$, $i=1,\dots,n$; i.e. uniform discretization is given in the lth iteration. In fact, the assumptions hold for $m=0$ and $l=0$. Then the scheme (3.14) has the following form:

$$
\begin{aligned}
(3.16)\quad &-\frac{1}{h^{m(l)}}\mathbf{r}_{i-1}^{m(l+1)}+\left(\frac{h^{m(l)}+h^m}{\Delta t}+\frac{2}{h^{m(l)}}\right)\mathbf{r}_i^{m(l+1)}-\frac{1}{h^{m(l)}}\mathbf{r}_{i+1}^{m(l+1)}\\
&\qquad=\frac{\mathbf{r}_{i-1}^m}{h^m}+\left(\frac{h^{m(l)}+h^m}{\Delta t}-\frac{2}{h^m}\right)\mathbf{r}_i^m+\frac{\mathbf{r}_{i+1}^m}{h^m}\,.
\end{aligned}
$$

If we set $a=\frac{h^{m(l)}+h^m}{\Delta t}+\frac{2}{h^{m(l)}}$, $b=-\frac{1}{h^{m(l)}}$, $d=\frac{h^{m(l)}+h^m}{\Delta t}-\frac{2}{h^m}$, and $e=\frac{1}{h^m}$, we obtain from (3.16) the cyclic tridiagonal system with constant coefficients (on the left- as well as on the right-hand side)

$$
(3.17)\qquad b\mathbf{r}_{i-1}^{m(l+1)}+a\mathbf{r}_i^{m(l+1)}+b\mathbf{r}_{i+1}^{m(l+1)}=e\mathbf{r}_{i-1}^m+d\mathbf{r}_i^m+e\mathbf{r}_{i+1}^m\,.
$$

Since the tridiagonal matrices are regular, from the eigenspace properties, it is clear that in the new iteration the vector $\mathbf{r}^{m(l+1)}$ represents again a uniformly discretized circle and thus $h_i^{m(l+1)} = h^{m(l+1)}$. By induction argument we get that at any time step and any iteration we get as a solution of the scheme the uniformly discretized circle.

Moreover, if $\mathbf{r}_i^m = r^m e^{\mathrm{i}\varphi}$ and $\mathbf{r}_i^{m(l+1)} = r^{m(l+1)} e^{\mathrm{i}\varphi}$, $i = 1, \dots, n$, then $r^{m(l+1)} = \lambda^{m(l+1)} r^m$ and $h^{m(l+1)} = 2r^{m(l+1)} \sin(\varphi/2) = \lambda^{m(l+1)} h^m$, because $h^m = 2r^m \sin(\varphi/2)$, and the scaling factor is given by the ratio of eigenvalues

$$\begin{aligned}\lambda^{m(l+1)} &= \frac{d + 2e\cos\varphi}{a + 2b\cos\varphi} = \frac{\frac{h^{m(l)}+h^m}{\Delta t} - \frac{2}{h^m}(1-\cos\varphi)}{\frac{h^{m(l)}+h^m}{\Delta t} + \frac{2}{h^{m(l)}}(1-\cos\varphi)} \\ &= \frac{\lambda^{m(l)}(\lambda^{m(l)}+1)(h^m)^2 - 2\Delta t\lambda^{m(l)}(1-\cos\varphi)}{\lambda^{m(l)}(\lambda^{m(l)}+1)(h^m)^2 + 2\Delta t(1-\cos\varphi)} \\ &= \frac{\lambda^{m(l)}(\lambda^{m(l)}+1)(r^m)^2 - \lambda^{m(l)}\Delta t}{\lambda^{m(l)}(\lambda^{m(l)}+1)(r^m)^2 + \Delta t}\end{aligned}$$

for $l = 0, 1, \dots$, where the relation $2\sin^2(\varphi/2) = (1 - \cos\varphi)$ was used in the last equality. Since $h^{m(0)} = h^m$, we define $\lambda^{m(0)} = 1$ as a starting point of such an iterative process representing our scheme for the uniformly discretized circle.

Let us define a function

$$g(\lambda) = \frac{\lambda(\lambda+1)(r^m)^2 - \lambda\Delta t}{\lambda(\lambda+1)(r^m)^2 + \Delta t}$$

for which $0 \le g(\lambda) < 1$ for $\lambda \in [0,1]$, $g(0) = 0$, and $g(1) < 1$. Among the positive numbers the mapping $\lambda \mapsto g(\lambda)$ has a fixed point $g(\lambda^*) = \lambda^*$, which is equal to

$$\lambda^* = \sqrt{1 - \frac{2\Delta t}{(r^m)^2}} \tag{3.18}$$

and is well defined if

$$\Delta t \le \frac{(r^m)^2}{2}. \tag{3.19}$$

Let us denote $c_1 = (r^m)^2$, $c_2 = \Delta t$. Then the derivatives of g have the form

$$g'(\lambda) = \frac{c_1 c_2 (1+\lambda)^2 - c_2^2}{(c_1\lambda(\lambda+1) + c_2)^2},$$

$$g''(\lambda) = \frac{1}{(c_1\lambda(\lambda+1)+c_2)^3}(-2c_1^2c_2 - 6c_1^2c_2\lambda - 6c_1^2c_2\lambda^2 - 2c_1^2c_2\lambda^3 + 4c_1c_2^2 + 6c_1c_2^2\lambda).$$

From the previous expressions it follows that provided $c_2 \le \frac{c_1}{2}$, which is nothing other than condition (3.19), the function g is increasing and concave in interval $[0,1]$. Then it is clear that the derivative of g must be strictly less than 1 in the interval $[\lambda^*, 1]$, which means that g is a contraction on that interval. Since we start the fixed point iterations by $\lambda = 1$, we get by the Banach fixed point theorem that our iterative process converges to the fixed point λ^*. This means that the solution of the scheme (3.13) at the new time step is the uniformly discretized circle with radius given by

$$r^{m+1} = \lambda^* r^m = \sqrt{(r^m)^2 - 2\Delta t}, \tag{3.20}$$

which for any Δt fulfilling the condition (3.19) coincides with the exact solution of the curve shortening problem (cf. (4.3)). ∎

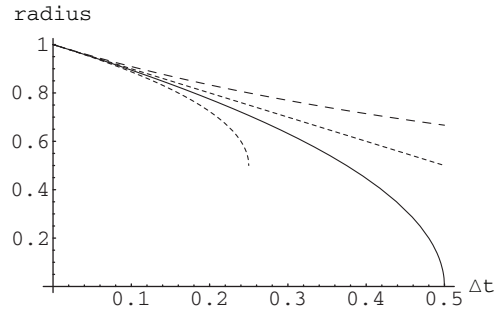

FIG. 3.1. *The curves representing dependence of the computed radius on the length of Δt for different schemes in case of evolving uniformly discretized circle. From the lowest to the highest curve: the fully implicit scheme, the higher order scheme (the bold curve), the explicit scheme, and the semi-implicit scheme.*

Remark 2. The statement in Theorem 3.1 does not hold for any of the explicit, semi-implicit, or fully implicit schemes. In fact, the reader can verify using the same strategy as above, that we have $r^{m+1} = r^m - \frac{\Delta t}{r^m}$ for the explicit scheme, $r^{m+1} = \frac{(r^m)^2}{r^m+\Delta t}$ for the semi-implicit scheme, and $r^{m+1} = \frac{r^m+\sqrt{(r^m)^2-4\Delta t}}{2}$ for the fully implicit scheme. Dependence of the error on the time step Δt in case of a unit circle is illustrated by Figure 3.1. The exact solution and solution by the higher order scheme coincide for any length of the time step $\Delta t \leq 1/2$, and the other schemes cannot be exact for any choice of time step. They are comparable for reasonably small time steps (see tables in the next section) and differ significantly in correct speed of shrinking when one would use large time steps (in which case the explicit forward Euler scheme can moreover be unstable).

THEOREM 3.2. *Let us consider* (1.4) *with $\varepsilon = 0$, $f = 0$ and with any constant tangential velocity α. Let the initial condition be given by a uniformly discretized circle. Then for any length of the time step Δt, the solution of the higher order scheme* (3.13) *remains on the same circle and distances of grid points do not change.*

Proof. Let the initial circle be given by complex numbers $\mathbf{r}_i^0 = r^0 e^{\mathbb{i}\varphi_i}$, $\varphi_i = i\varphi$, $\varphi = 2\pi/n$, $i = 1, \ldots, n$. Let us consider any cyclic antisymmetric tridiagonal matrix $\mathbf{A}$ with a diagonal coefficients equal to a, upper diagonal coefficients equal to -1, and lower diagonal coefficients equal to $+1$. By following calculations

$$e^{\mathbb{i}\varphi_{i-1}} + a e^{\mathbb{i}\varphi_i} - e^{\mathbb{i}\varphi_{i+1}} = \left(a + e^{-\mathbb{i}\varphi} - e^{\mathbb{i}\varphi}\right) e^{\mathbb{i}\varphi_i} = (a - 2\mathbb{i}\sin\varphi) e^{\mathbb{i}\varphi_i}, \tag{3.21}$$

we get that complex numbers representing grid points of the uniformly discretized circle are components of the eigenvector of matrix $\mathbf{A}$ with eigenvalue $\lambda_a = a - 2\mathbb{i}\sin\varphi$. In the same way we get that they are also components of the eigenvector for transpose matrix $\mathbf{A}^T$ with the complex conjugate eigenvalue $\lambda_a = a + 2\mathbb{i}\sin\varphi$.

Let us assume that $h_i^m = h$ and $h_i^{m(l)} = h$, where h is the distance of grid points of the uniformly discretized circle at the mth time step t^m. This assumption holds for $m = 0$ and $l = 0$. Then we can write the scheme (3.14) as follows:

$$\mathbf{r}_{i-1}^{m(l+1)} + \frac{4h}{\alpha\Delta t}\mathbf{r}_i^{m(l+1)} - \mathbf{r}_{i+1}^{m(l+1)} = -\mathbf{r}_{i-1}^m + \frac{4h}{\alpha\Delta t}\mathbf{r}_i^m + \mathbf{r}_{i+1}^m\,. \tag{3.22}$$

If we set $\frac{4h}{\alpha\Delta t} = a$, from the above-mentioned eigenspace properties, it is clear that the solution of (3.22) is given by

$$\mathbf{r}_i^{m(l+1)} = \lambda \mathbf{r}_i^m, \qquad i = 1, \ldots, n\,, \tag{3.23}$$

where

$$\lambda = \frac{\frac{4h}{\alpha\Delta t} + 2\mathbb{i}\sin\varphi}{\frac{4h}{\alpha\Delta t} - 2\mathbb{i}\sin\varphi} \tag{3.24}$$

is the eigenvalue of the matrix $\mathbf{A}^{-1}\mathbf{A}^T$. Using the fact that $|\lambda| = 1$, we see that all newly computed grid points stay on the circle with the same radius as in the mth time step. Since all position vectors $\mathbf{r}_i^m$ are multiplied by the same complex number λ, they all rotate by the same angle, and thus the distances between neighboring grid points do not change. The proof is finished by induction argument. □

Remark 3. Using the same strategy as above, we can write the result of the explicit forward Euler scheme in the form

$$\mathbf{r}_i^{m+1} = \left(\frac{4h}{\alpha\Delta t} + 2\mathbb{i}\sin\varphi\right)\mathbf{r}_i^m \tag{3.25}$$

and the result of the semi-implicit backward Euler scheme in the form

$$\mathbf{r}_i^{m+1} = \frac{1}{\left(\frac{4h}{\alpha\Delta t} - 2\mathbb{i}\sin\varphi\right)}\mathbf{r}_i^m\,. \tag{3.26}$$

In both cases the grid points remain on the same circle only if

$$\Delta t = \frac{4h}{\alpha\sqrt{1 - 4\sin^2\varphi}}\,. \tag{3.27}$$

4. Numerical experiments. First we present results concerning behavior of the scheme (3.13) in solving the curve shortening flow problem without the tangential redistribution (i.e., $\alpha = 0$) and without the driving force (i.e., $\mathbf{f} = 0$) in the evolution of a circle. We consider the circles with initial uniform distribution of grid points given by

$$x_i = \cos(2\pi i/n), \qquad y_i = \sin(2\pi i/n)\,, \tag{4.1}$$

as well as with initial nonuniform distribution of grid points given by

$$x_i = \cos(2\pi i/n + 0.125\sin(4\pi i/n)), \qquad y_i = \sin(2\pi i/n + 0.125\sin(4\pi i/n))\,, \tag{4.2}$$

$i = 1, \ldots, n$. We compare the accuracy of the schemes with the analytical solution, where the time dependent radius $|\mathbf{r}(t)|$ and area $A(t)$ of the shrinking circle are given by

$$|\mathbf{r}(t)| = \sqrt{\mathbf{r}(0)^2 - 2t} \tag{4.3}$$

and

$$A(t) = A(0) - 2\pi t. \tag{4.4}$$

The expression (4.4) holds for any curve evolving by curvature, and we will use it for testing precision of the schemes also in other examples. To estimate the error $e^M_{n(\mathbf{r})}$ in the radius, we use the numerical L_2 norm in the form

$$\left\|e^M_{n(\mathbf{r})}\right\| = \sqrt{\sum_{m=1}^{M}\Delta t\sum_{i=1}^{n}\left(|\mathbf{r}_i^m| - |\mathbf{r}(m\Delta t)|\right)^2\frac{h_i^m + h_{i+1}^m}{2}}\,, \tag{4.5}$$

and to estimate the error $e^M_{n(A)}$ in the area, we use the numerical L_2 norm in the form

$$\left\|e^M_{n(A)}\right\| = \sqrt{\sum_{m=1}^{M} \left(A^m - A(m\Delta t)\right)^2 \Delta t}\,, \tag{4.6}$$

where the curve encompassed area is given by

$$A^m = \frac{1}{2}\oint_\Gamma \mathbf{r}^m \cdot d\mathbf{r}^\perp \tag{4.7}$$

and the integral on the right-hand side is evaluated with higher order accuracy by using the fourth order Lagrange interpolation of points representing a discrete curve. We note that for a polygonal representation of a discrete curve, the formula (4.7) reduces to

$$A^m = \frac{1}{2}\sum_{i=1}^{n}(x_i y_{i+1} - x_{i+1} y_i), \tag{4.8}$$

and using (4.8) we would get similar results as reported in tables below, but we could not see a higher order accuracy of the new scheme as reported in the last column of Table 4.7.

For any of these quantities, the experimental order of convergence (EOC) is defined by

$$\mathrm{EOC} = \log_2 \frac{\left\|e^M_n\right\|}{\left\|e^{2M}_{2n}\right\|}\,. \tag{4.9}$$

For the experiments with shrinking circles we computed the errors in the time interval $[0, T]$ with $T = 0.1$, $|\mathbf{r}(0)| = 1$. We used $n = 10, 20, \ldots$ grid points and decreased correspondingly the time step Δt. The results for the explicit forward Euler and the semi-implicit backward Euler schemes are reported in Tables 4.1, 4.2, 4.3, and 4.4. We can see that both schemes are first-order accurate. For $n = 160$ and $\Delta t = 0.00625$ the stability of the explicit scheme is broken.

In Tables 4.5, 4.6, and 4.7, we show errors and EOC for the fully implicit backward Euler and our higher order scheme, where we used as stopping criterion for iterations $TOL = 10^{-8}$. While the fully implicit scheme is first-order accurate, the higher order scheme shows in this example fourth order accuracy when the grid points are nonuniformly distributed. For the uniformly discretized circle the errors drop to the machine precision limit (so we do not report EOC in this case), which is a consequence of the statement in Theorem 3.1.

In the next experiments we test our higher order scheme considering only tangential velocity without the curvature and driving force parts. The governing equation is then given by

$$\partial_t \mathbf{r} = \alpha \partial_s \mathbf{r}, \tag{4.10}$$

and our higher order scheme takes the form

$$\begin{aligned}\left(\frac{h^{m(l)}_{i+1} + h^{m(l)}_i + h^m_{i+1} + h^m_i}{\Delta t}\right)\mathbf{r}^{m(l+1)}_i + \alpha^{m(l)}_i \mathbf{r}^{m(l+1)}_{i-1} - \alpha^{m(l)}_i \mathbf{r}^{m(l+1)}_{i+1} \\ = \left(\frac{h^{m(l)}_{i+1} + h^{m(l)}_i + h^m_{i+1} + h^m_i}{\Delta t}\right)\mathbf{r}^m_i - \alpha^m_i \mathbf{r}^m_{i-1} + \alpha^m_i \mathbf{r}^m_{i+1}.\end{aligned} \tag{4.11}$$

TABLE 4.1

Numerical errors in radius and EOC for the shrinking unit circle with initial uniform and nonuniform distribution of grid points using the explicit forward Euler scheme.

		Uniform initial distribution		Nonuniform initial distribution	
n	Δt	$\left\|e^M_{n(\mathbf{r})}\right\|$	EOC	$\left\|e^M_{n(\mathbf{r})}\right\|$	EOC
10	1.0000e-1	4.381071e-3		4.383950e-3	
20	5.0000e-2	1.764560e-3	1.31197	1.764033e-3	1.31335
40	2.5000e-2	7.671827e-4	1.20166	7.670978e-4	1.20139
80	1.2500e-2	3.537897e-4	1.11667	3.537790e-4	1.11656
160	6.2500e-3	4.016483e-2	−6.8268	7.064467e-2	−7.6415

TABLE 4.2

Numerical errors in area and EOC for the shrinking unit circle with initial uniform and nonuniform distribution of grid points using the explicit forward Euler scheme.

		Uniform initial distribution		Nonuniform initial distribution	
n	Δt	$\left\|e^M_{n(A)}\right\|$	EOC	$\left\|e^M_{n(A)}\right\|$	EOC
10	1.0000e-1	9.732858e-3		9.603329e-3	
20	5.0000e-2	4.094604e-3	1.24914	4.079461e-3	1.23516
40	2.5000e-2	1.810195e-3	1.17758	1.809878e-3	1.17249
80	1.2500e-2	8.424295e-4	1.10352	8.424245e-4	1.10327
160	6.2500e-3	3.117283	−11.8534	3.392940e-2	−5.33184

TABLE 4.3

Numerical errors in radius and EOC for the shrinking unit circle with initial uniform and nonuniform distribution of grid points using the semi-implicit backward Euler scheme.

		Uniform initial distribution		Nonuniform initial distribution	
n	Δt	$\left\|e^M_{n(\mathbf{r})}\right\|$	EOC	$\left\|e^M_{n(\mathbf{r})}\right\|$	EOC
10	1.0000e-1	1.152790e-2		1.153664e-2	
20	5.0000e-2	4.929176e-3	1.22571	4.928358e-3	1.22704
40	2.5000e-2	2.217582e-3	1.15235	2.217372e-3	1.15225
80	1.2500e-2	1.041443e-3	1.09040	1.041413e-3	1.09030
160	6.2500e-3	5.031165e-4	1.04961	5.031127e-4	1.04958
320	3.1250e-3	2.470558e-4	1.02605	2.470553e-4	1.02604
640	1.5625e-3	1.223893e-4	1.01336	1.223892e-4	1.01335

TABLE 4.4

Numerical errors in area and EOC for the shrinking unit circle with initial uniform and nonuniform distribution of grid points using the semi-implicit backward Euler scheme.

		Uniform initial distribution		Nonuniform initial distribution	
n	Δt	$\left\|e^M_{n(A)}\right\|$	EOC	$\left\|e^M_{n(A)}\right\|$	EOC
10	1.0000e-1	2.608902e-2		2.590877e-2	
20	5.0000e-2	1.146247e-2	1.18652	1.144595e-2	1.17860
40	2.5000e-2	5.235098e-3	1.13063	5.234727e-3	1.12865
80	1.2500e-2	2.480186e-3	1.07777	2.480179e-3	1.07767
160	6.2500e-3	1.203856e-3	1.04279	1.203856e-3	1.04278
320	3.1250e-3	5.926125e-4	1.02250	5.926125e-4	1.02250
640	1.5625e-3	2.939439e-4	1.01155	2.939439e-4	1.01155

First we test motion of grid points along the circle with initial uniform distribution given by (4.1) in the time interval $\langle 0, 1\rangle$. We take the tangential velocity equal to constant $\alpha = 1$. To estimate the error in the radius $e^M_{n(\mathbf{r})}$, we use the numerical L_2

TABLE 4.5
Numerical errors in radius and EOC for the shrinking unit circle with initial uniform and nonuniform distribution of grid points using the fully implicit backward Euler scheme.

		Uniform initial distribution		Nonuniform initial distribution	
n	Δt	$\left\|e^M_{n(\mathbf{r})}\right\|$	EOC	$\left\|e^M_{n(\mathbf{r})}\right\|$	EOC
10	1.0000e-1	5.279112e-3		5.283129e-3	
20	5.0000e-2	1.928786e-3	1.4526	1.928205e-3	1.45413
40	2.5000e-2	8.011272e-4	1.26759	8.010384e-4	1.26732
80	1.2500e-2	3.614162e-4	1.14837	3.614053e-4	1.14825
160	6.2500e-3	1.711187e-4	1.07866	1.711174e-4	1.07863
320	3.1250e-3	8.318585e-5	1.04059	8.318569e-5	1.04058
640	1.5625e-3	4.100247e-5	1.02063	4.100245e-5	1.02063

TABLE 4.6
Numerical errors in area and EOC for the shrinking unit circle with initial uniform and nonuniform distribution of grid points using the fully implicit backward Euler scheme.

		Uniform initial distribution		Nonuniform initial distribution	
n	Δt	$\left\|e^M_{n(A)}\right\|$	EOC	$\left\|e^M_{(A)}\right\|$	EOC
10	1.0000e-1	1.284441e-2		1.301909e-2	
20	5.0000e-2	4.608831e-3	1.47867	4.625566e-3	1.49293
40	2.5000e-2	1.917708e-3	1.26502	1.918053e-3	1.26999
80	1.2500e-2	8.668743e-4	1.14549	8.668799e-4	1.14574
160	6.2500e-3	4.109380e-4	1.07690	4.109381e-4	1.07691
320	3.1250e-3	1.999022e-4	1.03963	1.999022e-4	1.03963
640	1.5625e-3	9.856638e-5	1.02013	9.856638e-5	1.02013

TABLE 4.7
Numerical errors in radius, area, and EOC for the shrinking unit circle with initial uniform and nonuniform distribution of grid points using the higher order scheme.

		Uniform initial	Nonuniform initial distribution			
n	Δt	$\left\|e^M_{n(\mathbf{r})}\right\|$	$\left\|e^M_{n(\mathbf{r})}\right\|$	EOC	$\left\|e^M_{n(A)}\right\|$	EOC
10	1.0000e-1	1.563145e-11	1.550446e-05		1.783068e-003	
20	5.0000e-2	2.175665e-12	1.060490e-06	3.86988	1.116485e-004	3.99733
40	2.5000e-2	6.527264e-13	6.192806e-08	4.09799	2.445996e-006	5.5124
80	1.2500e-2	3.411833e-13	3.630243e-09	4.09246	4.187014e-008	5.86836
160	6.2500e-3	5.330244e-14	2.178424e-10	4.05871	6.744933e-010	5.95597
320	3.1250e-3	2.268496e-14	1.332024e-11	4.03159	1.340712e-011	5.65273
640	1.5625e-3	1.020198e-15	8.228928e-13	4.01677	2.955194e-012	2.18167

norm in the form (4.5) where the exact solution is given by $|\mathbf{r}(m\Delta t)| = 1$ for all m and Δt. To estimate the error in angle we use

$$\left\|e^M_{n(\varphi)}\right\| = \sqrt{\sum_{m=1}^{M} \Delta t \sum_{i=1}^{n} \left(\varphi_i^m - \varphi_i(m\Delta t)\right)^2 \frac{h_i^m + h_{i+1}^m}{2}}, \tag{4.12}$$

where $\varphi_i^m = \arctan(\frac{y_i^m}{x_i^m})$ is the numerically computed angle and $\varphi_i(m\Delta t) = \frac{2\pi i}{n} + \alpha m\Delta t$ is the exact angle. To estimate the error in xth coordinate we use the norm

$$\left\|e^M_{n(x)}\right\| = \sqrt{\sum_{m=1}^{M} \Delta t \sum_{i=1}^{n} \left(x_i^m - x_i(m\Delta t)\right)^2 \frac{h_i^m + h_{i+1}^m}{2}}, \tag{4.13}$$

TABLE 4.8

Numerical error and EOC for the flow along unit circle with uniform initial distribution of grid points using the higher order scheme.

		Error in radius	Error in angle		Error in xth coordinate	
n	Δt	$\left\|e^M_{n(\mathbf{r})}\right\|$	$\left\|e^M_{n(\varphi)}\right\|$	EOC	$\left\|e^M_{n(x)}\right\|$	EOC
10	1.0000e-0	5.518289e-12	2.790356e-1		1.972044e-1	
20	5.0000e-1	3.180278e-12	6.265233e-2	2.15501	4.430032e-2	2.1543
40	2.5000e-1	1.621349e-12	1.405753e-2	2.15603	9.940152e-3	2.15598
80	1.2500e-1	8.149148e-13	3.270062e-3	2.10395	2.312283e-3	2.10395
160	6.2500e-2	4.051257e-13	7.845293e-4	2.05942	5.547460e-4	2.05942
320	3.1250e-2	2.020128e-13	1.918685e-4	2.03171	1.356715e-4	2.03171
640	1.5625e-2	1.007069e-13	4.742581e-5	2.01637	3.353511e-5	2.01637

TABLE 4.9

Numerical errors and EOC for the flow along circle with nonuniform initial distribution of grid points using the higher order scheme.

		Error in radius		Error in angle		Error in xth coordinate	
n	Δt	$\left\|e^M_{n(\mathbf{r})}\right\|$	EOC	$\left\|e^M_{n(\varphi)}\right\|$	EOC	$\left\|e^M_{n(x)}\right\|$	EOC
10	1.0000e-0	1.456888e-1		3.202141e-1		3.054001e-1	
20	5.0000e-1	4.001323e-2	1.86434	7.347136e-2	2.12378	7.349559e-2	2.05497
40	2.5000e-1	9.964680e-3	2.00558	1.658118e-2	2.14764	1.704088e-2	2.10866
80	1.2500e-1	2.409864e-3	2.04787	3.854981e-3	2.10475	4.003110e-3	2.08981
160	6.2500e-2	5.860890e-4	2.03976	9.235477e-4	2.06147	9.623525e-4	2.05648
320	3.1250e-2	1.440738e-4	2.02431	2.256523e-4	2.03308	2.353923e-4	2.03150
640	1.5625e-2	3.568771e-5	2.01331	5.573524e-5	2.01744	5.817354e-5	2.01663

TABLE 4.10

Numerical errors in radius and EOC for the flow along circle using nonconstant tangential velocity $\alpha(\varphi) = \sin(\varphi)$ and the higher order scheme.

		Uniform initial distribution		Nonuniform initial distribution	
n	Δt	$\left\|e^M_{n(\mathbf{r})}\right\|$	EOC	$\left\|e^M_{n(\mathbf{r})}\right\|$	EOC
10	2.000e-1	2.353631e-3		1.378267e-2	
20	1.000e-1	4.859034e-4	2.27615	3.084758e-3	2.15963
40	5.000e-2	1.016907e-4	2.25648	6.882263e-4	2.16420
80	2.500e-2	2.262966e-5	2.16790	1.598169e-4	2.10646
160	1.250e-2	5.293622e-6	2.09589	3.832247e-5	2.06016
320	6.250e-3	1.277208e-6	2.05126	9.370794e-6	2.03195
640	3.125e-3	3.134886e-7	2.02651	2.316119e-6	2.01646

where x_i^m is the numerically computed xth coordinate and $x_i(m\Delta t) = \cos(\frac{2\pi i}{n} + \alpha m\Delta t)$ is the exact coordinate. The results for the initial uniformly distributed unit circle are summarized in Table 4.8. In the next test we consider the initial nonuniform distribution of grid points given by (4.2). The exact solution for the angle is $\varphi_i(m\Delta t) = \frac{2\pi i}{n} + 0.2\sin(\frac{4\pi i}{n}) + \alpha m\Delta t$ and exact solution for the xth coordinate is $x_i(m\Delta t) = \cos(\frac{2\pi i}{n} + 0.2\sin(\frac{4\pi i}{n}) + \alpha m\Delta t)$. The results are summarized in Table 4.9.

Now we take variable tangential velocity $\alpha(\varphi) = \sin(\varphi)$ and we test the motion of grid points along the circle with initial uniform and nonuniform distribution of grid points given by (4.1) and (4.2) in the time interval $\langle 0, 2\rangle$. The results are summarized in Table 4.10.

TABLE 4.11

Numerical errors and EOC for the flow along ellipse using the higher order scheme with uniform velocity $\alpha = 1$ and nonuniform velocity $\alpha(\varphi) = \sin(\varphi)$.

		Uniform velocity		Nonuniform velocity	
n	Δt	$\left\|e^M_{n(\mathbf{r})}\right\|$	EOC	$\left\|e^M_{n(\mathbf{r})}\right\|$	EOC
10	1.0000e-0	5.958226e-2		5.953970e-2	
20	5.0000e-1	3.010777e-2	0.98475	1.384552e-2	2.10443
40	2.5000e-1	1.016811e-2	1.56608	3.111526e-3	2.15373
80	1.2500e-1	2.792546e-3	1.86440	7.133879e-4	2.12486
160	6.2500e-2	7.041488e-4	1.98763	1.683117e-4	2.08355
320	3.1250e-2	1.740029e-4	2.01677	4.069448e-5	2.04823
640	1.5625e-2	4.303869e-5	2.01541	9.993094e-6	2.02583

TABLE 4.12

Numerical area errors and EOC for the shrinking nonconvex curve using the higher order scheme without and with tangential redistribution (1.3) *with $\omega = 10$.*

		Without redistribution		With redistribution	
n	Δt	$\left\|e^M_{n(A)}\right\|$	EOC	$\left\|e^M_{n(A)}\right\|$	EOC
50	1.00e-3	crash		1.246709e-2	
100	1.00e-3	8.537182e-3		3.575597e-3	1.80187
200	5.00e-4	2.200680e-3	1.95581	9.528804e-4	1.90782
400	2.50e-4	5.548828e-4	1.98769	2.431527e-4	1.97043
800	1.25e-4	1.390618e-4	1.99646	6.111101e-5	1.99236

In the next experiment we test the motion of grid points along an ellipse with initial distribution given by

$$x_i = 2\cos(2\pi i/n), \qquad y_i = \sin(2\pi i/n). \tag{4.14}$$

We take again the constant tangential velocity $\alpha = 1$ and then also the nonuniform tangential velocity given by $\alpha(\varphi) = \sin(\varphi)$, in the time interval $\langle 0, 1\rangle$. To estimate the error we use the numerical L_2 norm in the form (4.5), where the exact radius is given by $|\mathbf{r}(x_i, y_i, m\Delta t)| = \sqrt{x_i^2/4 + y_i^2}$; i.e., it satisfies the equation of the ellipse. The results are summarized in Table 4.11.

Now let us consider the curve shortening flow solved by the higher order scheme (3.13) without and with the tangential grid points redistribution given by nontrivial tangential velocity (1.3). We computed the shrinking of a special nonconvex curve with the grid points given by

$$x_i = \cos(z), \qquad y_i = 0.5\sin(z) + \sin(x_i) + \sin(z)\left(0.2 + \sin(z)\sin^2(3z)\right), \tag{4.15}$$

$z = 2\pi i/n, i = 1, \ldots, n$. The results are summarized in Table 4.12 and in Figure 4.1. We can see that a suitable tangential redistribution reduces the area errors and makes the overall curve resolution better during the evolution. It also removes stability problems related to merging of grid points or creating swallow tails (which may cause a crash of computation), which is a usual drawback of naive Lagrangian approaches.

Finally, let us consider only the driving force part of (1.4), i.e.,

$$\partial_t \mathbf{r} = f\,(\partial_s \mathbf{r})^{\perp}\,. \tag{4.16}$$

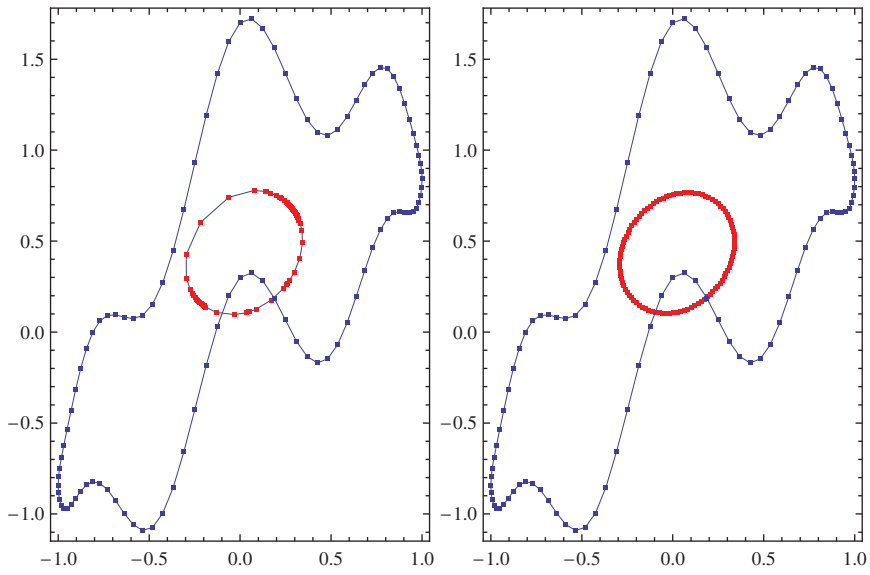

FIG. 4.1. *The shrinking nonconvex curve using the higher order scheme without (left) and with tangential redistribution* (1.3) *with* $\omega = 10$ *(right).*

Its discrete higher order form is given by

$$\frac{h_{i+1}^m + h_i^m + h_{i+1}^{m+1} + h_i^{m+1}}{2} \frac{\mathbf{r}_i^{m+1} - \mathbf{r}_i^m}{\Delta t} = f_i^m \left(\frac{\mathbf{r}_{i+1}^m - \mathbf{r}_{i-1}^m}{2} \right)^{\perp} + f_i^{m+1} \left(\frac{\mathbf{r}_{i+1}^{m+1} - \mathbf{r}_{i-1}^{m+1}}{2} \right)^{\perp},$$

and we solve iteratively the system of equations, which can be written for x and y coordinates in the following form:

$$\frac{h_{i+1}^{m(l)} + h_i^{m(l)} + h_{i+1}^m + h_i^m}{2\Delta t} x_i^{m(l+1)} = \frac{h_{i+1}^{m(l)} + h_i^{m(l)} + h_{i+1}^m + h_i^m}{2\Delta t} x_i^m + f_i^m \frac{y_{i-1}^m - y_{i+1}^m}{2} + f_i^{m(l)} \frac{y_{i-1}^{m(l)} - y_{i+1}^{m(l)}}{2},$$

$$\frac{h_{i+1}^{m(l)} + h_i^{m(l)} + h_{i+1}^m + h_i^m}{2\Delta t} y_i^{m(l+1)} = \frac{h_{i+1}^{m(l)} + h_i^{m(l)} + h_{i+1}^m + h_i^m}{2\Delta t} y_i^m + f_i^m \frac{x_{i+1}^m - x_{i-1}^m}{2} + f_i^{m(l)} \frac{x_{i+1}^{m(l)} - x_{i-1}^{m(l)}}{2}.$$

We test the above scheme in the evolution of uniformly and nonuniformly distributed initial unit circle using the evolving area error computed by (4.6), where the exact expression is given by $A(t) = \pi(\mathbf{r}_0 + ft)^2$. These errors for the expanding circle are reported in Table 4.13.

All the above discussed test examples show the second order accuracy of the higher order scheme in all particular parts of the intrinsic PDE (1.4). In the last numerical

TABLE 4.13
Numerical area errors and EOC for the expanding circle using the higher order scheme with uniform and nonuniform initial distribution of grid points.

		Uniform initial distribution		Nonuniform initial distribution	
n	Δt	$\left\|e^M_{n(A)}\right\|$	EOC	$\left\|e^M_{n(A)}\right\|$	EOC
10	1.0000e-1	9.400042e-003		9.179263e-003	
20	5.0000e-2	2.085962e-003	2.17195	2.162643e-003	2.08558
40	2.5000e-2	4.539989e-004	2.19995	4.938438e-004	2.13067
80	1.2500e-2	1.043818e-004	2.12082	1.141157e-004	2.11356
160	6.2500e-3	2.493888e-005	2.0654	2.727568e-005	2.06481

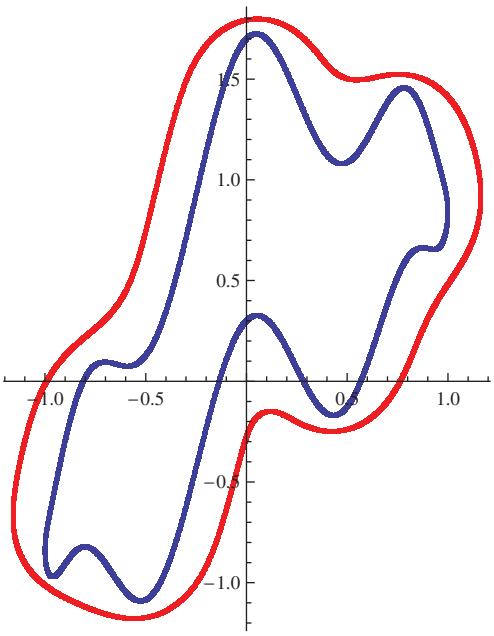

FIG. 4.2. *The initial nonconvex curve (blue points) and numerical solution at time step* 0.02 *(red points) of equation* (1.4) *with* $f = 10$, $\varepsilon = 1$, $\omega = 1$.

experiment we show that such accuracy brings a strong advantage of the higher order scheme in comparison with the other schemes regarding a balance between the CPU time and precision of computations. In Figure 4.2 we present evolution of the nonconvex curve (4.15) in general case $f = 10$, $\varepsilon = 1$, and $\omega = 1$ in time interval $\langle 0, 0.02\rangle$. In this test, we first computed the numerical solution by the semi-implicit scheme (3.4) using a very fine grid resolution, namely, with $n = 3200$, using subsequently divided time step Δt until the numerically computed area at the final time $T = 0.02$ did not change at the 7th valid digit; see Table 4.14. We obtained such a "gold standard" solution using $\Delta t = 4.882813 \times 10^{-8}$ and the area A was equal to 3.784484. The CPU time for such semi-implicit computation was 2053 s; cf. Table 4.14. The same "gold standard" solution was obtained by the higher order scheme (3.13) with a much larger time step $\Delta t = 1.25 \times 10^{-5}$ and consequently the CPU time was equal only to 22.25 s (cf. Table 4.14), which is almost 100 times faster. From the fifth column in Table 4.14 one can observe a second order in time accuracy of the higher order scheme for this spatially very fine grid.

TABLE 4.14

Report on CPU times in seconds and numerically computed enclosed area for different choices of time step Δt when using 3200 grid points in the semi-implicit backward Euler and the higher order schemes computing evolution of noncovex curve shown in Figure 4.2.

Semi-implicit scheme			Higher order scheme		
Δt	Area	CPU	Δt	Area	CPU
3.125000e-6	3.784438	2.740700e+1	8.00e-4	3.785275	9.1300e-1
1.562500e-6	3.784461	6.077900e+1	4.00e-4	3.784689	1.5980e+0
7.812500e-7	3.784473	1.293250e+2	2.00e-4	3.784536	2.4170e+0
3.906250e-7	3.784478	2.178270e+2	1.00e-4	3.784497	3.3970e+0
1.953125e-7	3.784481	4.170620e+2	5.00e-5	3.784487	8.7530e+0
9.765625e-8	3.784483	1.027939e+3	2.50e-5	3.784485	1.2167e+1
4.882813e-8	3.784484	2.053100e+3	1.25e-5	3.784484	2.2254e+1

5. Conclusions. In this paper we introduced a new higher order scheme for computing a tangentially stabilized curve shortening flow with a driving force. We proved that for any choice of time step this higher order scheme gives exact solution for evolving uniformly discretized circles in case of flow by curvature and in case of rotation by a constant tangential velocity. We have shown the second order accuracy and efficiency of the scheme on representative curve evolution examples.

REFERENCES

[1] S. B. ANGENENT AND M. E. GURTIN, *Multiphase thermomechanics with an interfacial structure 2. Evolution of an isothermal interface*, Arch. Ration. Mech. Anal., 108 (1989), pp. 323–391.

[2] M. BALAŽOVJECH AND K. MIKULA, *A higher order scheme for the curve shortening flow of plane curves*, in Proceedings of ALGORITMY 2009 - Conference on Scientific Computing, Podbanské, Slovakia, 2009, Publishing House of STU, Bratislava, Slovakia, 2009, pp. 165–175.

[3] J. W. BARRETT, H. GARCKE, AND R. NÜRNBERG, *On the variational approximation of combined second and fourth order geometric evolution equations*, SIAM J. Sci. Comput., 29 (2007), pp. 1006–1041.

[4] V. CASELLES, R. KIMMEL, AND G. SAPIRO, *Geodesic active contours*, Internat. J. Comput. Vision, 22 (1997), pp. 61–79.

[5] K. DECKELNICK, *Weak solutions of the curve shortening flow*, Calc. Var. Partial Differential Equations, 5 (1997), pp. 489–510.

[6] G. DZIUK, *Convergence of a semi discrete scheme for the curve shortening flow*, Math. Models Methods Appl. Sci., 4 (1994), pp. 589–606.

[7] G. DZIUK, *Discrete anisotropic curve shortening flow*, SIAM J. Numer. Anal., 36 (1999), pp. 1808–1830.

[8] M. GAGE AND R. S. HAMILTON, *The heat equation shrinking convex plane curves*, J. Differential Geom., 23 (1986), pp. 69–96.

[9] M. GRAYSON, *The heat equation shrinks embedded plane curves to round points*, J. Differential Geom., 26 (1987), pp. 285–314.

[10] T. Y. HOU, J. LOWENGRUB, AND M. SHELLEY, *Removing the stiffness from interfacial flows and surface tension*, J. Comput. Phys., 114 (1994), pp. 312–338.

[11] M. KASS, A. WITKIN, AND D. TERZOPULOS, *Snakes: Active contour models*, Internat. J. Comput. Vision, 1 (1987), pp. 321–331.

[12] S. KICHENASSAMY, A. KUMAR, P. OLVER, A. TANNENBAUM, AND A. YEZZI, *Conformal curvature flows: From phase transitions to active vision*, Arch. Rational Mech. Anal., 134 (1996), pp. 275–301.

[13] M. KIMURA, *Numerical analysis for moving boundary problems using the boundary tracking method*, Japan J. Indust. Appl. Math., 14 (1997), pp. 373–398.

[14] K. MIKULA AND J. KAČUR, *Evolution of convex plane curves describing anisotropic motions of phase interfaces*, SIAM J. Sci. Comput., 17 (1996), pp. 1302–1327.

[15] K. Mikula and D. Ševčovič, *Evolution of plane curves driven by a nonlinear function of curvature and anisotropy*, SIAM J. Appl. Math., 61 (2001), pp. 1473–1501.
[16] K. Mikula and D. Ševčovič, *A direct method for solving an anisotropic mean curvature flow of planar curve with an external force*, Math. Methods Appl. Sci., 27 (2004), pp. 1545–1565.
[17] K. Mikula and D. Ševčovič, *Computational and qualitative aspects of evolution of curves driven by curvature and external force*, Comput. Vis. Sci., 6 (2004), pp. 211–225.
[18] K. Mikula and D. Ševčovič, *Tangentially stabilized Lagrangean algorithm for elastic curve evolution driven by intrinsic Laplacian of curvature*, in Proceedings of ALGORITMY 2005 - Conference on Scientific Computing, Podbanské, Slovakia, 2005, Publishing House of STU, Bratislava, Slovakia, 2005, pp. 32–41.
[19] K. Mikula, D. Ševčovič, and M. Balažovjech, *A simple, fast and stabilized flowing finite volume method for solving general curve evolution equations*, Commun. Comput. Phys., 7 (2010), pp. 195–211.
[20] S. Osher and R. Fedkiw, *Level Set Methods and Dynamic Implicit Surfaces*, Springer, New York, 2003.
[21] W. H. Press, S. A. Teukolsky, W. T. Vetterling, and B. P. Flannery, *Numerical Recipes in C*, Cambridge University Press, Cambridge, 1992.
[22] J. A. Sethian, *Level set methods and fast marching methods. Evolving interfaces in computational geometry, fluid mechanics, computer vision, and materials science*, Cambridge Monogr. Appl. Comput. Math. 3, Cambridge University Press, Cambridge, 1999.
[23] D. Ševčovič and S. Yazaki, *Evolution of plane curves with a curvature adjusted tangential velocity*, Japan J. Indust. Appl. Math., to appear.
[24] S. Yazaki, *On the tangential velocity arising in a crystalline approximation of evolving plane curves*, Kybernetika (Prague), 43 (2007), pp. 913–918.